Demonstration of pseudo-ductility in unidirectional discontinuous carbon fibre/epoxy prepreg composites

Czél G., Pimenta S., Wisnom M. R., Robinson P.

Composites Science and Technology 106 (2015) 110–119

Contents lists available at ScienceDirect

Composites Science and Technology

journal homepage: www.elsevier.com/locate/compscitech

Demonstration of pseudo-ductility in unidirectional discontinuous carbon fibre/epoxy prepreg composites

Gergely Czél [a,*], Soraia Pimenta [b], Michael R. Wisnom [a], Paul Robinson [c]

[a] Advanced Composites Centre for Innovation and Science, University of Bristol, Queen's Building, Bristol BS8 1TR, United Kingdom
[b] The Composites Centre, Department of Mechanical Engineering, South Kensington Campus, Imperial College London, London SW7 2AZ, United Kingdom
[c] The Composites Centre, Department of Aeronautics, South Kensington Campus, Imperial College London, London SW7 2AZ, United Kingdom

ARTICLE INFO

Article history:
Received 29 April 2014
Received in revised form 20 October 2014
Accepted 25 October 2014
Available online 1 November 2014

Keywords:
Discontinuous-ply composites
B. Non-linear behaviour
B. Delamination
C. Damage mechanics
C. Stress transfer

ABSTRACT

The inherent brittleness of continuous unidirectional fibre reinforced composites is a major drawback to their otherwise outstanding mechanical performance. This paper exploits composites with overlapped discontinuities at the ply level to create a significantly non-linear response, due to progressive interlaminar damage under tensile loading. Two distinct configurations were manufactured with the same carbon/epoxy system and tested under quasi-static tension, showing that varying the thickness and length of the overlapping ply blocks resulted in significantly different mechanical responses and failure modes. A previously developed generalised shear-lag model was successfully used to optimise the overlap configuration, and accurately predicted the response in both strength- and toughness-dominated cases. This work demonstrates that unidirectional composites with well-designed discontinuities at the ply level can provide a significantly non-linear response with clear warning before failure, while retaining similar stiffness and up to 50% of the strength of their continuous counterparts.

1. Introduction

High performance carbon fibre composites offer exceptional stiffness- and strength-to-weight ratios, but suffer from sudden and brittle failure. There is usually very little or no warning before unstable failure and the residual load bearing capacity can be very poor. To ensure safe operation, a much greater safety margin is currently applied for composites than for more ductile materials such as metals, especially in critical applications. These design limitations can prevent engineers and operators from exploiting the outstanding stiffness and strength of carbon fibre composites, and render the materials unsuitable for applications in which loading conditions are not fully predictable and catastrophic failure cannot be tolerated. High performance composite materials that fail in a more ductile manner are therefore of exceptional interest and could potentially offer a substantial increase in the scope of applications, including transportation and civil engineering fields.

The study presented here aims at introducing pseudo-ductility into high performance fibre reinforced composites to make them suitable for new applications. One of the basic strategies to achieve pseudo-ductility is to create controlled failure mechanisms by modification of the architecture of the composite, e.g. by introducing designed ply discontinuities as in the test configuration shown in Fig. 1. This concept offers scope for pseudo-ductility through shearing and progressive failure of the interlaminar region in between ply discontinuities.

Some researchers have reported the use of discontinuous-ply composites for various purposes, ranging from mode II fracture testing to the improvement of hot forming capability of UD carbon prepregs. Cui et al. [1] executed central cut ply tests on UD glass/epoxy and carbon/epoxy composite specimens and studied the mode II fracture of the specimens. The effect of layer thicknesses and through thickness stresses on the fracture energy and delamination stress in tensile and compressive setups were highlighted. Wisnom and Jones [2] studied the delamination of UD composites plates with cut plies in four point bending as well, and successfully predicted the delamination stresses.

Matthams and Clyne [3,4] published a comprehensive study on the effect of laser-drilled holes on the tensile response of UD carbon/PEEK and carbon/PPS thermoplastic matrix composites. Various resulting fibre lengths in the range of 20–100 mm were investigated, and no decrease in elastic properties was observed, although a modest drop in tensile strength was reported. The deterioration of the structure and the drop in strength were reported to be acceptable for up to 25% tensile strain during hot forming.

* Corresponding author. Tel.: +44 (0) 117 33 15311; fax: +44 (0) 117 95 45360.
E-mail address: G.Czel@bristol.ac.uk (G. Czél).

http://dx.doi.org/10.1016/j.compscitech.2014.10.022
0266-3538/

Iarve and Kim [5,6] studied and predicted the failure parameters of UD staggered discontinuous carbon/epoxy tow composites. The reported dominant failure mechanisms were (i) longitudinal splitting along the 5 mm wide tows (in 25 mm wide specimens) and (ii) in-plane delamination of tows.

Yashiro and Ogi [7] studied the tensile behaviour of cross ply laminates with slits in the 0° plies at different angles. Transverse cracking and delamination were reported to start from the crossing point of the slits and splitting was also observed on the boundaries of the damaged area. Taketa et al. [8] reported that introducing designed slits in standard UD carbon prepregs can improve the formability of the material during hot pressing. This new approach can provide better material properties than sheet moulding compound (SMC) hot pressing technology, exploiting the better alignment of fibres. Li et al. [9] developed the so-called unidirectionally arrayed chopped strands (UACS) further by introducing new slit patterns to improve the strength, material symmetry and flowability.

Baucom et al. [10] studied UD carbon/epoxy composite plates including some continuous plies and zones where most of the plies were cut. Cut patterns were optimised to retain strength for 1:3 continuous-to-cut ply ratios. 92% of the strength of the continuous baseline specimens was retained with the best proposed cut pattern.

Malkin et al. [11] used cut ply prepreg composites to achieve a gradual and controlled failure in UD carbon specimens under 4 point bending.

Heim et al. [12] tested three layer UD discontinuous ply specimens similar to the five layer one shown in Fig. 1. They attempted to determine the critical fibre length of carbon/carbon composites using these double lap joint type specimens.

All the above cited authors were analysing UD composites with various objectives. Feraboli et al. [13,14] investigated the structure and the damage modes of randomly oriented chopped carbon/epoxy prepreg tapes using an ultrasound imaging technique. The randomly oriented chopped tapes were reported to make the composite material virtually notch-insensitive, but sensitive to specimen size due to the heterogeneous meso-structure.

Our scope was different from those of the studies in the literature, with the final aim of exploring possible ways of adding pseudo-ductile characteristics to high performance UD carbon/epoxy composites. The key challenge of the work was to demonstrate a novel concept through a realistic model system which provides ductility in the form of a non-linear stress–strain response and clear warning before failure, while maintaining high initial stiffness. The understanding of the factors controlling the dominant failure modes was our objective as well. A previously developed modelling tool [15] was used for designing optimised specimens and interpreting the results.

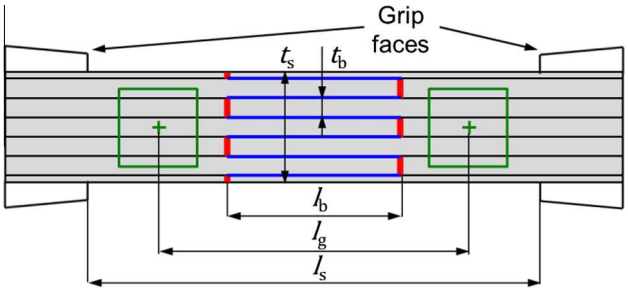

Fig. 1. Side view schematic of the discontinuous ply composite configuration (red lines show discontinuities, blue lines show the load transferring sheared interfaces green boxes show the targets for optical strain measurement). (For interpretation of the references to colour in this figure legend, the reader is referred to the web version of this article.)

2. Specimen design

The basic concept of the study was the use of discontinuous (cut) UD prepreg plies laid up in blocks in an overlapped architecture (see Fig. 1), to create a zone in the middle of the tensile specimens where the tensile load is transferred by shear stresses at the ply block interfaces. The goal was to achieve a nonlinear stress–strain response, with high initial modulus followed by a significant loss of stiffness due to interlaminar damage, before final failure. Two specimen types were designed with different models. The *short overlap* design was suggested using a very basic calculation assuming uniform shear stress along the overlaps. The optimised *long overlap* specimen was designed using a previously developed shear-lag model which considers the full non-linear response (including failure) of the interface between the ply blocks [15].

2.1. Materials

The material considered in this study is IM7/8552, an aerospace grade UD carbon/epoxy prepreg system supplied by Hexcel Co., Ltd. with 0.125 mm cured ply thickness [16], 200 g/m^2 and 134 g/m^2 masses per unit area for prepreg and dry fibres respectively, and 57.7% nominal fibre volume fraction. Hexcel 8552 is a toughened 180 °C cure epoxy resin system and IM7 fibres are intermediate modulus carbon fibres with an elastic modulus of 276 GPa and strain to failure of 1.9%. Table 1 shows the mechanical properties of the cured IM7/8552 prepreg composites.

2.2. Preliminary calculations assuming uniform shear stresses along the ply block interfaces

In order to design UD cut ply composite specimens with non-linear response, it was initially imposed that interlaminar shear failure should occur before ply block fracture. The design criterion was formulated by equating (i) the total force due to uniform shear stresses on the interfaces to (ii) the total force arising from tensile stresses in the continuous ply blocks, at the moment of shear failure of the interfaces:

$$\frac{n_{IL} l_b S_{IL}}{t_s - t_d} = \sigma_{cont} < X_b, \tag{1}$$

where n_{IL} is the number of interfaces between the ply blocks, l_b is the overlap length, t_s is the full thickness of the specimen (as shown in Fig. 1), t_d is the total thickness of the discontinuous ply blocks in the weakest cross section (which is at the right series of layer discontinuities in Fig. 1, assuming surface ply blocks of less than half the inner block thickness), S_{IL} is the interlaminar shear strength of the composite (between the ply blocks), X_b is the tensile strength of the composite in the fibre direction, and σ_{cont} is the tensile stress in the continuous ply blocks at (shear) failure. This simple criterion assumes a uniform distribution of shear stresses along the overlap areas, which is a notable simplification; nevertheless, the equation is still applicable as a first check for thick and rigid ply blocks and relatively short overlaps, where the actual shear stress distribution is expected to be relatively uniform.

The *short overlap* type specimen was designed to have a large safety margin against ply block fracture, using 8 plies within a block except for the surface blocks which had only 2 plies; this reduction is necessary as the surface layers are much more susceptible to delamination. Firstly, there is only one delaminating interface for these blocks, effectively doubling the mode-II energy release rate (if they were to have the same thickness as the inner blocks). Secondly, there is a mode-I component which "peels off" the surface layers. Reducing the surface ply block thickness from 8 to 2 plies should be sufficient to avoid premature delamination

Table 1
Properties of IM7/8552 cured UD composite (the terms in brackets indicate the coefficients of variation of the test data in%).

Cured ply thickness (mm)	Longitudinal tension		Matrix shear modulus, G_{IL} (GPa) [17]	Interlaminar		Resin rich thickness, t_{IL} (mm) [a]
	Modulus, E_b (GPa) [16]	Strength, X_b (MPa) [16]		Shear strength, S_{IL} (MPa) [18]	Fracture toughness, $\mathcal{G}_{IIc.IL}$ (kJ/m^2) [19]	
0.125	164	2724	1.5	82.5 (5.7)	0.79 (10.1)	0.005

[a] Assumed for modelling.

Table 2
Nominal geometries of the tested specimen types (see Fig. 1 for notations, all dimensions in mm).

Specimen type	Inner ply block thickness, t_b	Surface ply block thickness	Nominal overlap length, l_b	Specimen thickness, t_s	Gauge length, l_g	Free length, l_s	Width, W_s
Short overlap	1.0	0.25	4	5.5	8	15	20
Long overlap	0.25	0.125	8	1.5	10	12	20

initiating there. The parameters of the specimen designs can be found in Table 2. Substituting the specified geometrical parameters, $n_{IL} = 6$, $l_b = 4$ mm, $t_d = 3$ mm (see definitions above) and the interlaminar shear strength from Table 1, Eq. (1) gives an estimated maximum fibre direction stress $\sigma_{cont} = 792$ MPa in the continuous ply blocks in the critical cross section, which is well below the tensile strength of the composite, even allowing for stress concentrations around the discontinuities. The basic calculation indicates that this setup is very likely to produce an interlaminar shear failure on the overlapped interfaces, without any layer fracture. The predicted average tensile stress at failure across the whole thickness is only 360 MPa, but this is acceptable since it is intended to be a model configuration.

2.3. Optimised design using a generalised shear-lag model considering non-linear interlaminar response with interlaminar fracture

2.3.1. Overview of modelling approach

It has been shown [15] that, in order to fully exploit the potential for ductility and non-linear response in discontinuous composites, it is necessary to consider the whole constitutive law (including fracture) of the interlaminar phase under shear. Classical approaches, relying on a single parameter (interfacial shear strength or mode-II fracture toughness) to characterise the response of the matrix or interface, are valid only for extreme cases of the overlap aspect-ratio $\alpha = l_b/t_b$. Strength-dominated models (based on perfect plasticity, as described in Section 2.2) are accurate for low aspect-ratios, while toughness-dominated formulations (based on linear elastic fracture mechanics, LEFM) are valid for high aspect-ratios.

The analytical shear-lag model for discontinuous composites with 'brick-and-mortar' architecture and generic matrix response developed by Pimenta and Robinson [15] is here used to optimise the configuration of the discontinuous-ply specimen shown in Fig. 1 for maximum ductility and non-linear behaviour. The model considers a composite with regularly staggered stiff 'platelets' embedded in a soft 'matrix'. It assumes a piecewise linear but otherwise completely generic shear constitutive law for the 'matrix', which is consistent with a defined fracture toughness; this is used to model the 'interlaminar phase' in this paper (hereafter identified by the subscript IL). The 'platelets' are assumed to be linear-elastic until failure, and are used to represent the ply blocks (hereafter identified by the subscript b, with stiffness E_b and strength X_b) in the paper.

The model analyses a unit-cell of the staggered composite (representing one single overlap between two ply blocks shown in Fig. 1) under tensile loading, using a shear-lag formulation (in which stresses in the overlap zone are transferred between ply blocks by shearing of the interlaminar phase); the overall strain is calculated as the predicted extension over the overlap zone divided by its initial length [15].

2.3.2. Predictions for the mechanical response of shear overlaps

The generalised shear-lag model [15] was applied to the IM7/8552 carbon/epoxy system, with nominal properties defined in Table 1. The interlaminar phase was modelled with a bi-linear constitutive law, which is suitable for very thin interphases (as it was verified that there was virtually no resin rich zone between the ply blocks in the specimens tested) made of relatively brittle materials (as it is the case of the 8552 epoxy, with bulk tensile failure strain below 5% [17]). The interlaminar constitutive law was defined by the matrix shear modulus G_{IL} (from literature [17]), interlaminar shear strength S_{IL} (measured experimentally [18] through double notched shear tests), and mode-II interlaminar fracture toughness $\mathcal{G}_{IIc.IL}$ (measured experimentally [19] through four point bending end notched flexure tests). The interlaminar thickness t_{IL} was assumed to be similar to the fibre diameter [16], as previous parametric studies [15] showed that t_{IL} has virtually no influence on the response of discontinuous composites modelled with a bi-linear matrix. The resulting interlaminar constitutive law is shown in Fig. 2.

The model assumes half thickness for the surface ply blocks due to symmetry considerations, although the surface ply block thickness of the *short overlap* specimens was only one quarter of the inner ply block thickness.

Fig. 3 shows the predicted equilibrium stress–strain responses of the overlap zones, considering nominal properties but different overlap geometries; ply block thicknesses were increased incrementally according to the cured ply thickness of the IM7/8552 prepreg. For relatively small overlap aspect-ratios (α), the interlaminar damage process zone (DPZ) occupies the full length of the overlap, but the condition of zero shear stress (indicating the onset of interlaminar fracture) is not reached prior to the predicted maximum stress (except for the largest value of α for $t_b = 0.5$ mm, where interlaminar fracture occurs just before final failure). For these cases, both strength and extension at failure increase with increasing α (see Fig. 3a and b). The *short overlap configuration* (l_b and t_b defined in Section 2.2 and Table 2) is predicted to have limited strength and strain to failure (as shown in Fig. 3a), even though non-linearity initiates at very low applied stresses (highlighted as □).

For overlaps with aspect-ratios high enough to accommodate the entire interlaminar damage process zone (DPZ), a crack tip is formed under load (highlighted as ○ in Fig. 3c and d) and propagates under constant remote stresses. For a given ply block thickness t_b, the

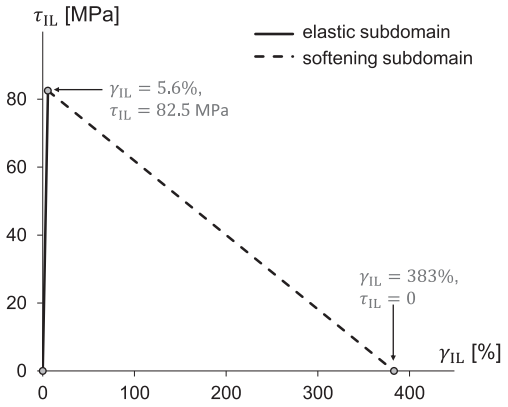

Fig. 2. Shear-stress vs. shear-strain constitutive law of the interlaminar phase assumed in the generalised shear-lag model.

stress for crack initiation is independent of the aspect-ratio α (see Fig. 3c and d); further increasing the overlap length l_b reduces the strain at crack initiation and extends the crack propagation plateau. Thinner ply blocks require larger aspect-ratios and higher stresses for crack initiation (for instance, an interlaminar crack forms if $\alpha = 16$ and $t_b = 0.5$ mm, but not if $\alpha = 16$ and $t_b = 0.25$ mm, see Fig. 3b and c). The *long overlap* configuration highlighted in Fig. 3c was selected for experimental testing (see full geometry definition in Table 2), because it maximises non-linearity and is safe against ply fracture.

The effect of varying interlaminar properties on the predicted response of the two selected configurations is shown in Fig. 4. This highlights that the response of the *short overlap* is dominated by the interfacial shear strength, while that of the *long overlap* is dominated by the mode-II fracture toughness (previous Finite Element (FE) analyses [15] showed that there is a small mode-I component in the surface ply blocks of the specimen represented in Fig. 1, but for relatively thin ply blocks this is a local effect with a small influence on the overall response, see Section 4.1). Small variations of interlaminar properties should have no influence on the qualitative response of both configurations.

3. Experimental

A detailed description of specimen types, manufacturing, test methods and tensile test results is given in this section. The specimen geometries selected during the design phase are given in Table 2.

3.1. Specimen manufacturing

The new type composites involving discontinuous prepreg plies needed new manufacturing procedures, especially to make sure that the cuts do not affect the performance of the fibres around them, and that they are aligned accurately during lay-up. A 25 mm diameter "pizza wheel" blade was found to be suitable to make the sensitive internal cuts, because the shearing of the fibre

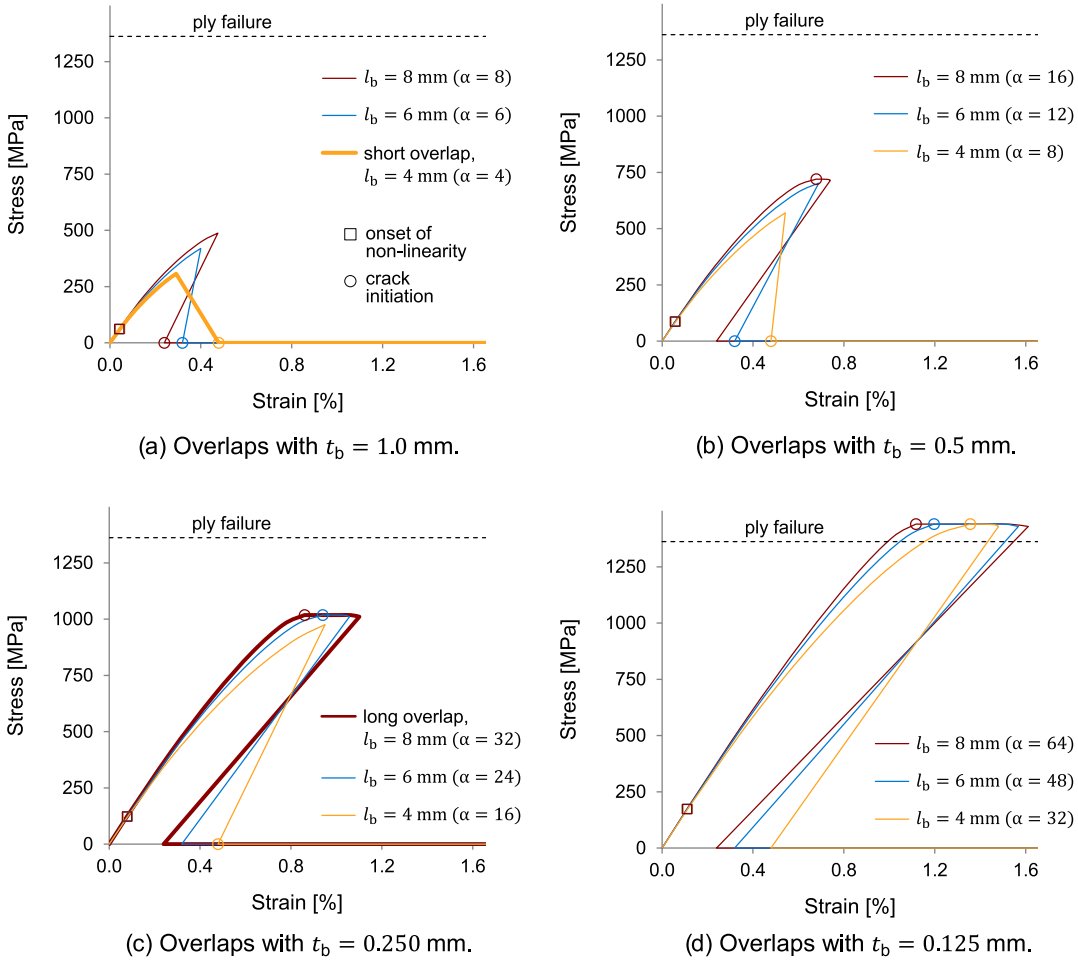

Fig. 3. Predicted stress–strain curves considering different overlap zone geometries. The responses of the nominal configurations to be tested (*short overlap* and *long overlap*) are highlighted by thick lines.

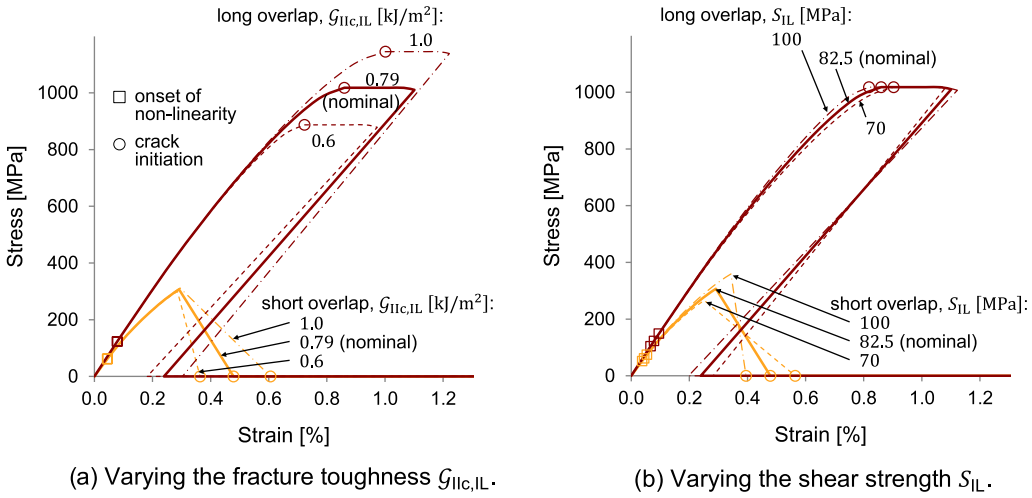

Fig. 4. Predicted stress–strain curves for the nominal configurations to be tested (*short overlap* and *long overlap*), considering different interlaminar properties in the overlap zones.

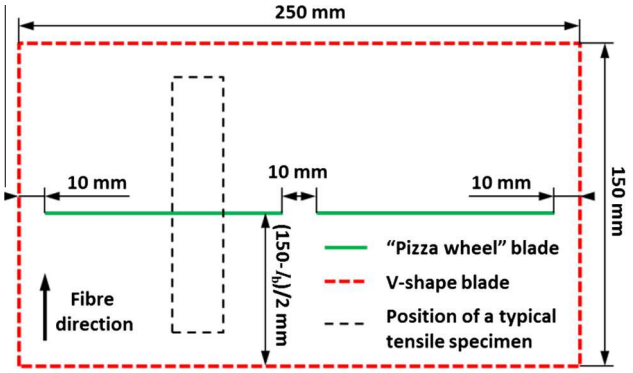

Fig. 5. Geometry and cut pattern of the individual plies.

ends can be avoided this way. The steps of the manufacturing route for the cut blocked ply specimens were the following:

1. Creating the internal cuts on the uncured prepreg sheet with a 25 mm diameter "pizza wheel" blade on a CNC ply cutter to fabricate the overlap zone (see Fig. 5);
2. Cutting the uncured prepreg plies with a standard V-shape blade on a CNC ply cutter to the size of the plate to be manufactured (see Fig. 5);
3. Laying up the ply blocks while carefully aligning one edge of the cut plies;
4. Stacking the discontinuous ply blocks together to create the discontinuity pattern shown in Fig. 1;
5. Bagging up the composite plate using a suitable size silicone frame around the composite to prevent thinning of the plate towards the edges due to resin bleed-out. A stiff top plate (e.g. a 2–3 mm thick Al plate) was also necessary to prevent the composite plate thinning around the overlap zone;
6. Curing the composite laminate in an autoclave using the recommended cure cycle (2 h @180 °C and 0.7 MPa) [16];
7. Fabrication of individual specimens with a diamond cutting wheel.

Fig. 6a shows the resulting alignment of discontinuities on a longitudinal section micrograph for a typical *short overlap* type specimen. It can be seen that the alignment of the individual plies is good but not perfect, resulting in small steps within the boundaries of the resin pockets. The width of the resin pockets is around 0.5 mm and the resulting average overlap length is 3.71 mm. Fig. 6b shows a typical longitudinal section of a *long overlap* type specimen at a similar scale as that of Fig. 6a to enable visual assessment of the overlap zone geometries. The measured average overlap length of the *long overlap* type specimens is 7.64 mm, more than twice as high as that of the *short overlap* type specimens.

3.2. Test method

The testing of cut blocked ply UD carbon/epoxy composite specimens was executed under uniaxial tensile loading and displacement control with a crosshead speed of 0.2 mm/min on an Instron 8801 type 100 kN rated servo-hydraulic computer controlled universal test machine. Strains were measured using an Imetrum video gauge system. Strains were measured on the edge of each specimen, because the discontinuities made it unsuitable to measure strains on the specimen faces. Gauge lengths for both specimen types were set to be just above the overlap lengths to focus on the response of the overlap zones (see Table 2).

Fig. 7a shows the overall test setup for the *short overlap* specimens with a high power studio light positioned overhead, which guaranteed enough light in between the grip faces for good quality optical strain measurements. In the case of the *long overlap* specimens, the setup shown in Fig. 7a resulted in a greater scatter in the strain data, most probably because these specimens were much more sensitive to any small misalignment than the *short overlap* ones. The strains were therefore measured simultaneously on both vertical edges of the *long overlap* specimens and then averaged to compensate for any possible misalignment in the load string. Fig. 7b shows the test setup for *long overlap* specimens with double cameras.

3.3. Results and discussion

Fig. 6c and d shows that both specimen types exhibited the designed failure type and fractured along the sheared interfaces with no significant fibre damage.

3.3.1. Short overlap type specimens

Fig. 8a shows typical tensile stress–strain curves of a *short overlap* type specimen. Fig. 8a shows two curves because the resin pockets (visible in Fig. 6) cracked at around half of the final failure

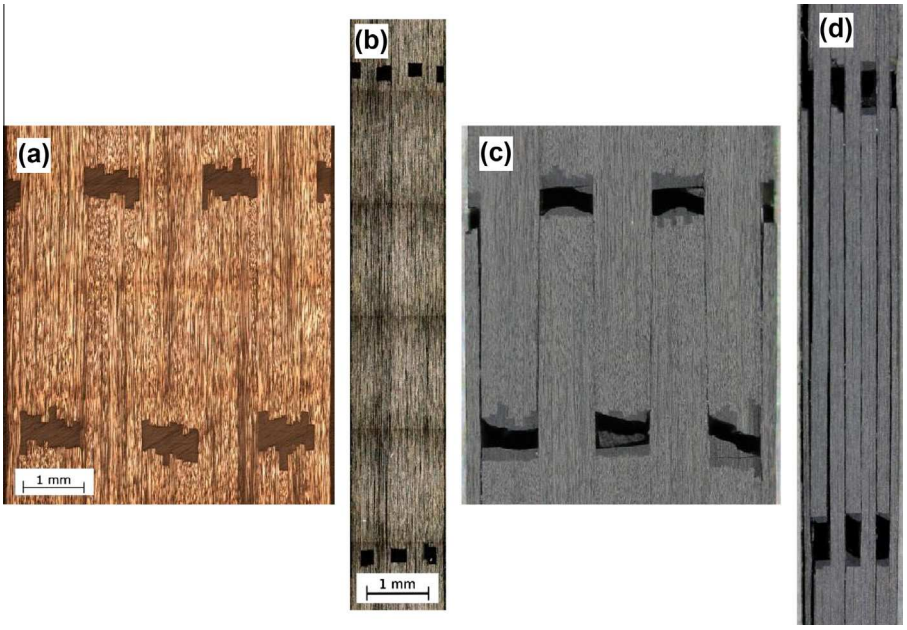

Fig. 6. Similar scale typical longitudinal section micrographs of (a) *short overlap*, (b) *long overlap* type specimens and edge view photographs of failed, (c) *short overlap*, and (d) *long overlap* type specimens.

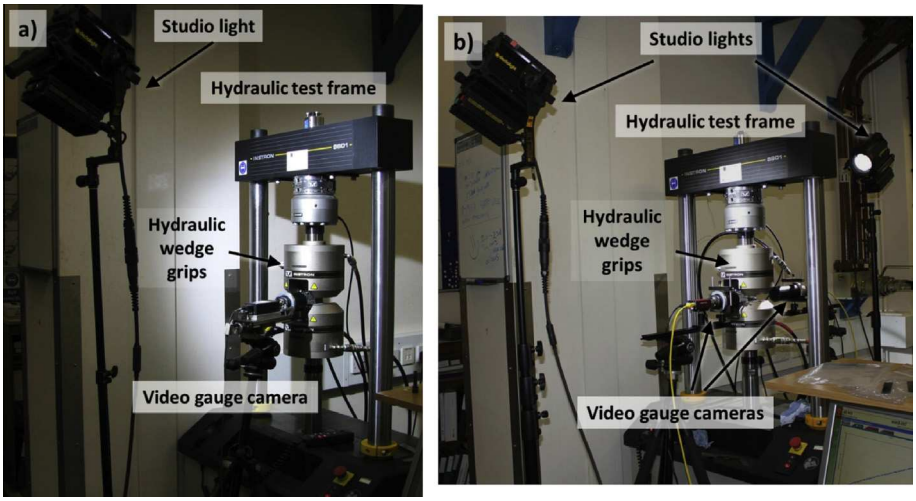

Fig. 7. Tensile test setups with (a) single video gauge, and (b) double video gauges .

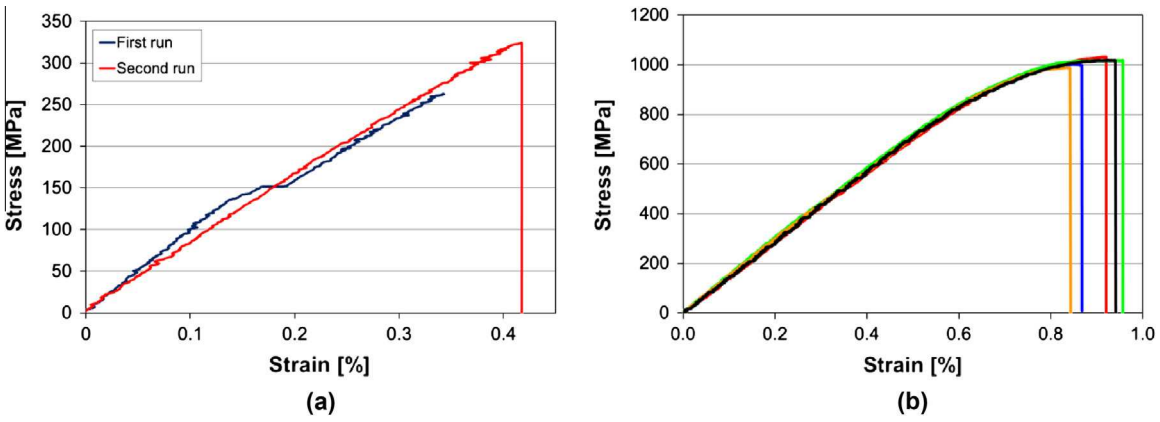

Fig. 8. Typical stress–strain curves of (a) *short overlap*, and (b) *long overlap* type specimens.

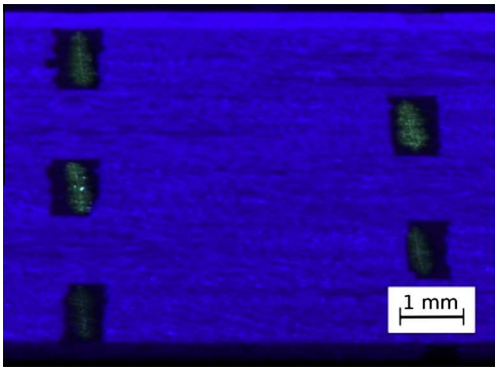

Fig. 9. Micrograph of a *short overlap* type specimen taken under UV light after an interrupted test and dye penetration (green patches show the UV dye coming out of the resin pocket cracks). (For interpretation of the references to colour in this figure legend, the reader is referred to the web version of this article.)

load, causing a horizontal shift and a notable change in the stiffness of the specimens. This effect was highlighted by stopping the test at around the 80% of the failure load, unloading the specimen and re-loading it to final failure in a second run. Fig. 9 shows the resin pocket cracking on an interrupted test specimen after applying UV dye.

The *short overlap* type specimens showed limited strength and extension to failure and overall agreed well with the predictions of the simple equation (Section 2.2) and the generalised shear-lag formulation (Section 2.3). An updated prediction for *short overlap* specimens using the measured average $l_b = 3.71$ mm in Eq. (1) gives an expected average failure stress of 334 MPa across the whole plate thickness, which is very close to the measured 322 MPa average strength of the specimens. This indicates that the assumption of uniform shear stresses on the interfaces in the overlap zone is reasonable.

3.3.2. Long overlap case

Fig. 8b shows the stress–strain graphs of five *long overlap* type specimens, where strains correspond to the average of the strains measured on both edges of each specimen. Table 3 shows the summary of the test results.

The most important differences between the two specimen types are their different ply block thicknesses and overlap lengths, which resulted in different failure types and stress–strain responses. The *long overlap* type specimens failed in a favourable way, showing a significantly non-linear stress–strain response before final failure and stress plateaus for some of the specimens. The maximum stress and strain of this specimen type was significantly improved by the longer overlap lengths and the resulting much higher *total sheared interface area/specimen cross sectional area* ratio, but the achievable maximum stress was limited by interlaminar crack initiation. As a result of the higher tensile stresses in the ply blocks, the mode-II energy release rate became high enough to cause significant interlaminar damage, while the *long overlap* provided enough residual load transfer capacity.

The strain measurement videos of those specimens exhibiting a stress plateau suggest that interlaminar cracks initiated at the side of the specimen with resin pockets on the surface (at the set of discontinuities shown on the left side of Fig. 1). No delamination was observed on the specimens showing no stress plateau. The resolution of the videos was however not high enough to allow for any further analysis of the damage process (e.g. interlaminar cracking sequence or crack length determination, etc). In the case of the *long overlap* type specimens, the resin pockets also failed earlier than final failure (confirmed by the videos), but this was a minor damage event not detectable on the stress–strain graphs.

4. Comparison between experimental and modelling results

4.1. Overall stress–strain response

Fig. 10 compares modelling and experimental stress–strain curves for the discontinuous-ply specimens. Predictions were obtained using the generalised shear-lag formulation [15], and considering a bi-linear matrix response represented in Fig. 2. Nominal properties are shown in Table 1; since the experimental determination of interlaminar properties (especially S_{IL} and $\mathcal{G}_{IIc,IL}$) is complex and still under discussion in the literature [20], the effect of possible deviations of interlaminar properties is also analysed in Fig. 10. The effective overlap length l_b for each configuration was taken as the average measured experimentally (Table 3), and all other geometric parameters are given in Table 2.

Two geometric details of the *short overlap* specimens deviated from the assumptions of the original generalised shear-lag model for composites with 'brick-and-mortar' architecture [15]. On one hand, the thickness of the outer ply blocks was ¼ of the thickness of the inner blocks in the experiments (and not ½ as assumed in the model). On the other hand, relatively large resin pockets (see Fig. 6) increased the compliance of the specimens. To account for the latter effect, predicted strains were corrected according to the equation below (in which the first term corresponds to the overlap zone and the second term accounts for ply extension at the resin pockets):

$$\varepsilon_{\infty}^{corr} = \varepsilon_{\infty} \cdot \frac{l_g - 2 \cdot l_m}{l_g} + \frac{2 \cdot \sigma_{\infty}}{E_b} \cdot \frac{2 \cdot l_m}{l_g}, \quad (2)$$

where $l_m = 0.5$ mm is the length of each resin pocket, ε_{∞} is the predicted strain and σ_{∞} is the predicted longitudinal stress in the gross section.

The agreement between modelling and experiments for the *short overlap* case (Fig. 10a) is reasonably good; both tested and predicted stress–strain curves show little non-linearity. Differences in the stiffness and strength may be due to (i) the mismatch in the thickness of the outer plies and presence of resin pockets (see above), and (ii) the fact that the experimental curves correspond to re-testing partially loaded specimens (hence some stiffness degradation is expected, see Section 3.3.1). The predicted unloading equilibrium path is not seen in the experiments, likely due to the extra compliance generated by the free length of the specimen and testing setup (which may lead to snap-back in the overlap zone under remote displacement control).

Table 3
Tensile test results (The terms in brackets indicate the coefficients of variation of the test data in %).

Specimen type	Number of specimens tested	Measured overlap length, l_b (mm)	Ply block thickness, t_b (mm)	Initial modulus (first run) (GPa)	Failure stress (MPa)	Strain to failure (%)
Short overlap	5	3.71	1.0	103.0 (8.8)	322 (3.2)	0.37 (8.7)
Long overlap	5	7.64	0.25	148.7 (2.4)	1009.6 (1.7)	0.905 (5.3)

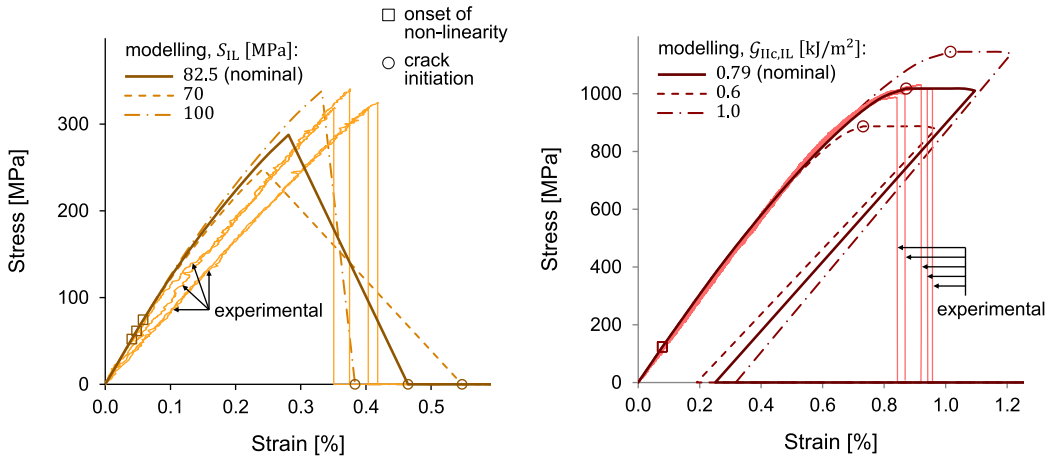

(a) *Short overlap* configuration (corrected according to Eq. 2).

(b) *Long overlap* configuration.

Fig. 10. Modelling predictions and experimental results for the stress–strain curves of discontinuous-ply specimens.

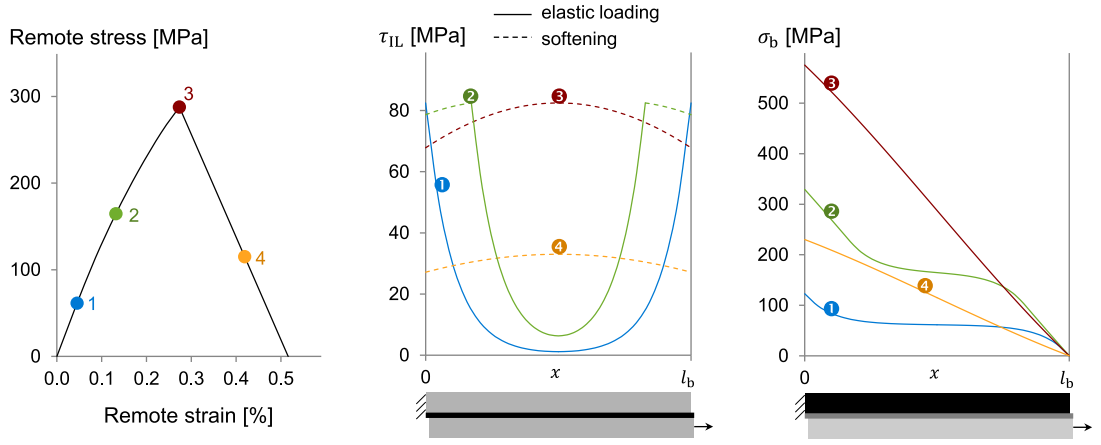

(a) Stress-strain curve for the *short overlap*. Points 1-4 correspond to the fields in b)-c).

(b) Interlaminar shear stresses within the overlap length, for the points highlighted in a).

(c) Ply tensile stresses within the overlap length, for the points highlighted in a).

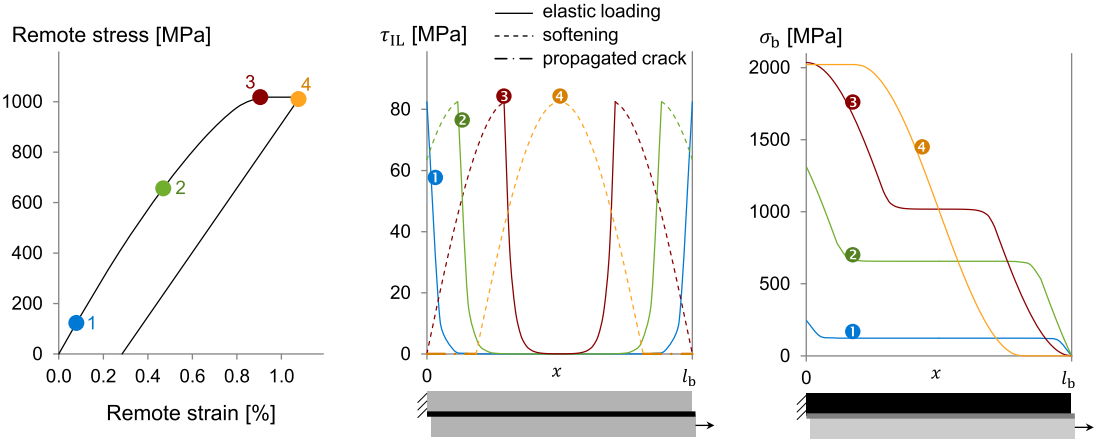

(d) Stress-strain curve for the *long overlap*. Points 1-4 correspond to the fields in e)-f).

(e) Interlaminar shear stresses within the overlap length, for the points highlighted in d).

(f) Ply tensile stresses within the overlap length, for the points highlighted in d).

Fig. 11. Evolution of stress fields (from the generalised shear-lag model) in a *short overlap* (a–c) and a *long overlap* (d–f).

The *long overlap* configuration was designed strictly according to the generalised shear-lag model, and optimised for non-linearity of the stress–strain curve. The agreement between modelling and experiments shown in Fig. 10b is remarkably good. Experimental failure occurred approximately at the stress and strain predicted for crack initiation (highlighted as ○), considering the nominal fracture toughness of $\mathcal{G}_{\mathrm{IIc,IL}} = 0.79\,\mathrm{kJ/m^2}$. Previous parametric studies [15] showed that the fracture toughness is the main interlaminar property governing the response of *long overlaps*, with the effect illustrated in Fig. 10b; on the contrary, the interlaminar shear strength, interlaminar thickness and shape of the interlaminar constitutive law have a negligible effect on the overall stress–strain response of the overlapping region [15].

Only 2 of the 5 tested *long overlap* specimens exhibited a stress plateau after the predicted onset of delamination and the observed plateaus were shorter than that predicted by the model. FE analyses [15] suggest that this was caused by (i) small variations of local material properties (especially interlaminar fracture toughness and/or shear strength) and of the lengths of the six overlaps within a specimen (leading to premature failure governed by the weakest overlap), and (ii) a small (one third) mode-I component of the energy release rate at the outer plies (leading to premature failure due to mixed-mode delamination). The equilibrium unloading path could not be captured under remote displacement control, due to snap-back in the overlap zone.

Fig. 10 validates the ability of the generalised shear-lag model to predict stress–strain curves for discontinuous-ply configurations with non-ductile interlaminar phase, for both strength- and toughness-dominated cases. Moreover, the model allowed the successful design of an overlap configuration with significantly non-linear response, as evidenced by the progressive stiffness degradation down to a nearly-zero tangent value in the *long overlap* case.

4.2. Analysis of deformation mechanisms

Fig. 11 shows the evolution of stress fields in the overlap zone with remote loading. When the *short overlap* reaches the maximum overall stress (curve ❸ in Fig. 11c), interlaminar shear stresses are nearly constant, and the tensile stress profile in the plies is quasi-linear. This justifies why the strength of the *short overlap* is dominated by the interlaminar shear strength, and can be accurately modelled through a perfectly-plastic formulation (Eq. (1)). Interlaminar degradation (i.e. softening) initiates at point ❶, but no crack tip is expected to be fully formed even when the overall tangent stiffness becomes negative (see curve ❹ in Fig. 11b).

The evolution of interlaminar stresses in the *long overlap* (Fig. 11e) shows that the central part of the overlap does not transmit stresses during the entire loading phase (see $\tau_{\mathrm{IL}} \approx 0$ in curves ❶, ❷ and ❸). At point ❸, the interlaminar DPZ is fully developed ($\tau_{\mathrm{IL}} \in [0, S_{\mathrm{IL}}]$), and two crack tips are formed at $x = 0$ and $x = l_b$; the corresponding stress (σ_a) coincides with that predicted by LEFM for crack propagation,

$$\sigma_a = \sqrt{\frac{2 \cdot E_b \cdot \mathcal{G}_{\mathrm{IIc,IL}}}{t_b}}. \tag{3}$$

Subsequently, the cracks propagate towards the centre of the overlap, until the interlaminar phase loses its ability to transfer load in the elastic domain (point ❹) and overall failure occurs.

4.3. Optimised configuration and limitations

It has been shown previously [15] that, for shear overlaps with thin and non-ductile interlaminar phase, the optimal configuration (superscript $*$) for maximum strength and ductility is defined by:

$$t_b^* = \frac{8 \cdot E_b \cdot \mathcal{G}_{\mathrm{IIc,IL}}}{X_b^2} \quad \text{and} \quad l_b^* = \frac{\pi \cdot \sqrt{t_b^* \cdot E_b \cdot \mathcal{G}_{\mathrm{IIc,IL}}}}{\sqrt{2} \cdot S_{\mathrm{IL}}}, \tag{4}$$

where the optimal ply block thickness t_b^* leads to interlaminar crack initiation at the stress for ply failure, and the overlap length l_b equals twice the interlaminar DPZ length. The corresponding strength and failure strain of the optimised configuration are [15]:

$$X^* = \frac{X_b}{2} \quad \text{and} \quad e^* = \frac{X_b}{E_b} \cdot \left(\frac{1}{\pi} + \frac{1}{2}\right). \tag{5}$$

For the mechanical properties shown in Table 1,

$$\begin{cases} t_b^* = 0.140\ \mathrm{mm} \\ l_b^* = 3.62\ \mathrm{mm} \end{cases} \quad \text{and} \quad \begin{cases} X^* = 1362\ \mathrm{MPa} \\ e^* = 1.36\% \end{cases}. \tag{6}$$

The strain to failure of the optimised configuration is predicted to be lower than that of the conventional UD material (see Eq. (5)). Nevertheless, the predicted non-linear response (see similar configuration in Fig. 3d with $\alpha = 32$) does provide warning before failure. This improves the inspectability of composites without sacrificing their initial stiffness, which could promote the reduction of safety factors used in the design of composite structures.

5. Conclusions

The following conclusions were drawn from the presented study of unidirectional discontinuous overlapped ply carbon/epoxy composites:

- Pseudo-ductility has been demonstrated in a discontinuous UD carbon/epoxy prepreg composite material, showing significantly non-linear and predictable overall stress–strain response. Similar initial modulus to that of continuous fibre reinforced specimens was achieved, and a reasonably high maximum stress (above 1000 MPa) was reached after a significant reduction in tangent stiffness towards zero, allowing for damage detection and load redistribution before final failure.
- The generalised shear-lag model proposed by Pimenta and Robinson [15] was successfully applied to design an overlap configuration combining high non-linearity before final failure with high stiffness and strength. The good agreement between modelling and experiments – for both strength- and toughness-dominated configurations – validates the formulation for composites with 'brick-and-mortar' architecture with non-ductile interlaminar phase.
- A novel manufacturing technique involving "pizza wheel" blade ply cutting and a unique cut design was developed for the discontinuous blocked ply unidirectional carbon/epoxy laminates, producing very well controlled discontinuities in the model specimens.
- The two tested specimen configurations produced different stress–strain responses because of different overlap zone geometries. In the *short overlap* case, the thick ply blocks resulted in a very long damage process zone (DPZ), making the interlaminar shear stresses in the overlap zone relatively uniform, but preventing any interlaminar crack initiation; this led to an interfacial strength driven failure at low applied stress and strain, due to the *short overlap*. On the contrary, the geometry of the *long overlap* case allowed for interlaminar crack initiation, as (i) the ply blocks were thin, which decreased the DPZ length, and (ii) the overlap was

long enough to transfer high tensile stresses to the ply blocks and to accommodate the full interlaminar DPZ. This resulted in high mode-II energy release rates in the overlap zone, allowing for crack initiation on the interfaces in some specimens before final failure.

- The non-linear response in the *long overlap* configuration was achieved by optimising the ply block thickness (to trigger a crack tip at stresses near those required for ply failure) and the overlap length (to accommodate the entire interlaminar damage process zone). While the potential for further improvements using thin and brittle interfaces is limited (see Section 4.3), a ductile and thicker interlaminar phase could increase failure strains of discontinuous-ply specimens through extensive yielding (rather than fracture).

Acknowledgement

This work was funded under the EPSRC Programme Grant EP/I02946X/1 on High Performance Ductile Composite Technology.

References

[1] Cui W, Wisnom MR, Jones MI. An experimental and analytical study of delamination of unidirectional specimens with cut central plies. J Reinf Plast Compos 1994;13:722–39.
[2] Wisnom MR, Jones MI. Delamination of unidirectional glass fibre–epoxy with cut plies loaded in four point bending. J Reinf Plast Compos 1995;14:45–59.
[3] Matthams TJ, Clyne TW. Mechanical properties of long-fibre thermoplastic composites with laser drilled microperforations. 1. Effect of perforations in consolidated material. Compos Sci Technol 1999;59:1169–80.
[4] Matthams TJ, Clyne TW. Mechanical properties of long-fibre thermoplastic composites with laser drilled microperforations. 2. Effect of prior plastic strain. Compos Sci Technol 1999;59:1181–7.
[5] Iarve EV, Kim R. Three-dimensional fracture analysis and experimental investigation of model unidirectional discontinuous tow composite laminates. J Thermoplast Compos Mater 2002;15:469–76.
[6] Iarve EV, Kim R. Strength prediction and measurement in model multilayered discontinuous tow reinforced composites. J Compos Mater 2004;38:5–18.
[7] Yashiro S, Ogi K. Fracture behavior in CFRP cross-ply laminates with initially cut fibers. Compos Part A: Appl Sci Manuf 2009;40:938–47.
[8] Taketa I, Okabe J, Kitano A. A new compression-molding approach using unidirectionally arrayed chopped strands. Compos Part A: App Sci Manuf 2008;39:1884–90.
[9] Li Hang, Wang Wen-Xue, Takao Yoshihiro, Matsubara Terutake. New designs of unidirectionally arrayed chopped strands by introducing discontinuous angled slits into prepreg. Compos Part A: Appl Sci Manuf 2013;45:127–33.
[10] Baucom JN, Thomas JP, Pogue WR, Qidwai Siddiq M. Tiled composite laminates. J Compos Mater 2010;44:3115–32.
[11] Malkin R, Yasaee M, Trask R, Bond I. Bio-inspired laminate design exhibiting pseudo-ductile (graceful) failure during flexural loading. Compos Part A: Appl Sci Manuf 2013;54:107–16.
[12] Heim D, Hartmann M, Neumayer J, Klotz C, Ahmet-Tsaous Ömer, Zaremba S, et al. Novel method for determination of critical fiber length in short fiber carbon/carbon composites by double lap joint. Compos Part B: Eng 2013;54:365–70.
[13] Feraboli P, Cleveland T, Ciccu M, Stickler P, DeOto L. Defect and damage analysis of advanced discontinuous carbon/epoxy composite materials. Compos Part A: Appl Sci Manuf 2010;41:888–901.
[14] Feraboli P, Peitso E, Cleveland T, Stickler PB, Halpin JC. Notched behavior of prepreg-based discontinuous carbon fiber/epoxy systems. Compos Part A: Appl Sci Manuf 2009;40:289–99.
[15] Pimenta S, Robinson P. An analytical shear-lag model for composites with 'brick-and-mortar' architecture considering non-linear matrix response and failure. Compos Sci Technol 2014;104:111–24.
[16] <http://www.hexcel.com/Resources/DataSheets/Prepreg-Data-Sheets/8552_eu.pdf>; [accessed 18.10.13].
[17] Kaddour AS, Hinton MJ, Smith PA, Li S. Mechanical properties and details of composite laminates for the test cases used in the third world-wide failure exercise. J Compos Mater 2013;47(20–21):2427–42.
[18] May M, Hallett SR. An assessment of through-the-thickness shear tests for initiation of fatigue failure. Compos Part A: Appl Sci Manuf 2010;41:1570–8.
[19] Camanho PP, Maiami P, Davila CG. Prediction of size effects in notched laminates using continuum damage mechanics. Compos Sci Technol 2007;67:2715–27.
[20] Schuecker C, Davidson BD. Evaluation of the accuracy of the four-point bend end-notched flexture test for mode II delamination toughness determination. Compos Sci Technol 2000;60:2137–46.